Nano Research
2019, 12(12): 3031–3036

ISSN 1998-0124 CN 11-5974/O4
https://doi.org/10.1007/s12274-019-2548-8

Research Article

One-step synthesis of thermally stable artificial multienzyme cascade system for efficient enzymatic electrochemical detection

Xiqing Cheng[1], Jinhong Zhou[1], Jiayu Chen[1], Zhaoxiong Xie[1,2], Qin Kuang[1] (✉), and Lansun Zheng[1]

[1] *State Key Laboratory of Physical Chemistry of Solid Surfaces, Collaborative Innovation Center of Chemistry for Energy Materials, and Department of Chemistry, College of Chemistry and Chemical Engineering, Xiamen University, Xiamen 361005, China*
[2] *Pen-Tung Sah Institute of Micro-Nano Science and Technology, Xiamen University, Xiamen 361005, China*

Received: 10 September 2019 / **Revised:** 6 October 2019 / **Accepted:** 17 October 2019

ABSTRACT

Recently, metal-organic framework (MOF)-based multienzyme systems integrating different functional natural enzymes and/or nanomaterial-based artificial enzymes are attracting increasing attention due to their high catalytic efficiency and promising application in sensing. Simple and controllable integration of enzymes or nanozymes within MOFs is crucial for achieving efficient cascade catalysis and high stability. Here, we report a facile electrochemical assisted biomimetic mineralization strategy to prepare an artificial multienzyme system for efficient electrochemical detection of biomolecules. By using the GO*x*@Cu-MOF/copper foam (GO*x*@Cu-MOF/CF) architecture as a proof of concept, efficient enzyme immobilization and cascade catalysis were achieved by *in situ* encapsulation of glucose oxidase (GO*x*) within MOFs layer grown on three-dimensional (3D) porous conducting CF via a facile one-step electrochemical assisted biomimetic mineralization strategy. Due to the bio-electrocatalytic cascade reaction mechanism, this well-designed GO*x*@Cu-MOF modified electrode exhibited superior catalytic activity and thermal stability for glucose sensing. Notably, the activity of GO*x*@Cu-MOF/CF still remained at ca. 80% after being incubated at 80 °C. In sharp contrast, the activity of the unprotected electrode was reduced to the original 10% after the same treatment. The design strategy presented here may be useful in fabricating highly stable enzyme@MOF composites applied for efficient photothermal therapy and other platform under high temperature.

KEYWORDS

metal-organic frameworks, artificial multienzyme, electrochemical assisted biomimetic mineralization, glucose detection, thermal stability

1 Introduction

Enzymatic catalysis, which often involves multienzyme cascade reactions, has been widely applied in the synthesis of pharmaceuticals and fine chemicals [1, 2], biofuel cells [3, 4], biocatalysis [5, 6], and biosensing [7, 8] due to the high efficiency and selectivity of natural enzymes [9]. However, the application of enzymatic catalysis is still hampered by the poor stability of enzymes. Consequently, many researchers have focused on enhancing the multienzyme catalytic reaction by integrating different functional natural or artificial enzyme catalysts in a well-designed reactor [5, 10–12]. In such multienzyme systems, enzyme catalysis processes can be individually or completely replaced by highly stable nanomaterials with enzyme-like characteristics (nanozymes) [13–15]. Benefiting from the combination of enzymes and nanozymes, the activity of cascade catalysis and the stability of enzyme can be significantly improved. However, the overall performance of multienzyme systems is not only affected by the specific interactions among catalysts, substrates and reactor, but also by other factors, such as substrate channeling, kinetics matching, and spatial distribution in reactor [16]. Therefore, rational engineering of the multienzyme system architecture is the key to efficient cascade catalysis and high stability.

Recently, metal-organic frameworks (MOFs) with regular pores or channels have garnered considerable research interest due to their excellent potential as a universal platform for the immobilization of various functional materials including enzymes and nanozymes [5–8, 11, 12, 17–26]. High flexibility and tunability of MOFs in terms of their pore size and shape allow the encapsulation of catalysts with different sizes and functions in specific spaces for efficient cascade reaction [27–29]. Unfortunately, MOF-based multienzyme systems as a new research field is facing a huge challenge both in the aspects of its construction and technology at present. First, simple and controllable integration of enzymes and nanozymes within MOFs is still very difficult due to great differences in composition, activity and stability between enzymes and nanozymes as well as their affinity with MOFs [30]. Furthermore, when applied to enzyme modified electrodes for biosensing, the MOF encapsulation strategy for enzyme immobilization meets great challenges in controlling the mass/electron transport between the immobilized natural/artificial enzymes and the conducting electrode, which significantly influences efficient cascade between enzyme/nanozyme-catalyzed reactions and sensitive signal acquisition [31–35].

Herein, using the GO*x*@Cu-MOF/copper foam (GO*x*@Cu-MOF/CF) based electrochemical biosensor as a proof of concept, a novel natural enzyme and nanozyme cascade catalysis strategy was proposed to establish a sensitive and stable electrochemical biosensor for detection of glucose. In this multienzyme system, glucose oxidase (GO*x*) was immobilized within Cu-based MOF (HKUST-1/Cu-MOF) layers grown on the surface of three-dimensional (3D) porous conducting copper foam electrode via a facile electrochemical assisted biomimetic mineralization. The ordered porous structure of Cu-MOF not only facilitates the diffusion of substrates/products onto/from

Address correspondence to qkuang@xmu.edu.cn

active sites, but also effectively protects the enzyme from the effects of harsh conditions (e.g. high temperature), thereby significantly improving their stability and durability in practical sensing processes.

2 Experimental

2.1 Chemicals and materials

Copper foam used as electrochemical deposition substrate was purchased from Shenzhen Tiancheng Technology Co., Ltd. (China). 1, 3, 5-Benzenetricarboxylic acid ($C_9H_6O_6$, BTC) was purchased from Sigma-Aldrich. Methanol (CH_3OH), hydrochloric acid (HCl), sodium phosphate dibasic dehydrate ($NaH_2PO_4{\cdot}2H_2O$) and disodium hydrogen phosphate dodecahydrate ($Na_2HPO_4{\cdot}12H_2O$) was obtained from Sinopharm Chemical Reagent Co., Ltd. (China). Glucose oxide (BR, 100–250 U/mg) was purchased from Shanghai Yuanye Bio-Technology Co., Ltd. All chemicals were directly used after purchase without further purification. All the solutions were prepared with a Millipore Milli-Q system.

2.2 Preparation of GO*x*@Cu-MOF/CF

Prior to the experiment, the copper foam was first immersed in dilute hydrochloric acid for 1 min to remove the oxide on the surface. Then, the copper foam was immersed thoroughly in water and treated ultrasonically for 10 min. Finally, the copper foam was washed with water to neutral and dried in air. In a typical experiment, 8 mM BTC (17.2 mg) was dissolved in 4 mL methanol. A separate solution of 10 mg GO*x* dissolved in 6 mL phosphate solution was also prepared. Then the two solutions were mixed, and the resulting solution was used as the electrolyte solution. The synthesis of GO*x*@Cu-MOF onto copper foam was carried out on electrochemical workstation (CHI1130B, Chenhua, Shanghai) at 1.0–2.0 V with magnetic agitation at room temperature. A saturated calomel electrode (SCE), platinum wire, and copper foam served as reference, counter electrodes, and working electrode, respectively. The same method was used to prepare other GO*x*@Cu-MOF modified electrodes, except for deposition times, deposition potentials or concentrations (GO*x* and of BTC).

2.3 Characterization of sample

High-resolution scanning electron microscope (FE-SEM, HITACHI-S4800, Japan), and transmission electron microscopy (TEM, Tecnai F30, USA, 300 kV) equipped with energy-dispersive X-ray (EDX) spectroscopy were first employed to characterize morphology and microstructures of the GO*x*@MOF/copper foam and the GOx@MOFs. The phases of the samples were investigated via powder X-ray diffraction (PXRD) patterns acquired with a Panalytical X-pert diffractometer using Cu Kα radiation (λ = 1.5418 Å, 40 kV, 40 mA, scanning rate: 0.25°/s) in the range of 5°–80°. The Fourier transform infrared (FTIR) spectroscopy was recorded in the solid state as KBr dispersion using Thermo Nicolet 380 FT-IR spectrometer.

2.4 Electrochemical measurements

The electrochemical performance of the GO*x*@MOF modified electrodes and the activity of GO*x* were evaluated using an electrochemical workstation (CHI1130B, Chenhua, Shanghai) with a conventional three-electrode system, including a Pt wire as the counter electrode, SCE as reference electrode, and GO*x*@MOF/CF as working electrode. The working electrode was first activated with cyclic voltammetry (CV) in 0.1 mol/L PBS solution (pH 7.4) until a steady CV was acquired. The activity is calculated by the current density increment of 4 mM glucose.

3 Results and discussion

Scheme 1 illustrates the proposed protocol for the fabrication of

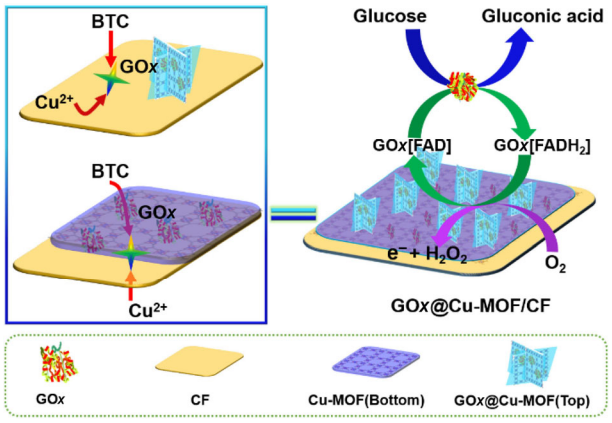

Scheme 1 The protocol for GOx immobilization with Cu-MOF on copper foam and bio-electrocatalytic cascade reaction mechanism towards glucose sensing.

GO*x*@Cu-MOF/CF and the cascade catalytic mechanism for glucose sensing. The GO*x*@Cu-MOF modified copper foam (denoted as GO*x*@Cu-MOF/CF) was fabricated via a one-step electrochemical assisted biomimetic mineralization process. In this synthetic process, the GO*x* was electrostatically adsorbed onto the copper foam substrate (denoted as GO*x*/CF) (Fig. S1 in the Electronic Supplementary Material (ESM)). Due to the enzyme-induced biomineralization effect, Cu-MOFs that were formed by electrochemically dissolved Cu^{2+} ions from the copper foam and organic ligands (such as 1, 3, 5-benzenetricarboxylic acid) in the solution gradually nucleated and grew around GO*x*, finally forming GO*x*@Cu-MOF encapsulation structure on the copper foam [36–38]. By constructing this architecture, the detection of glucose can be efficiently realized via a cascade reaction process between glucose oxidation catalyzed by GO*x* and hydrogen peroxide reduction electrocatalyzed by Cu-MOF/ CF electrode. In essence, this bio-electrocatalytic detection process of glucose simulates the bi-enzymatic cascade catalytic reaction of glucose oxidase and catalase [13]. The open and porous 3D feature of the copper foam provides enhanced specific surface area for enzyme immobilization and facilitates the substrate transport and charge collection. Another advantage of the architecture is that the encapsulation structure provides good protection for GO*x*.

The representative low-magnification SEM images of the as-prepared GO*x*@Cu-MOF modified copper foam at a potential of 1.5 V (vs. SCE) for 1,200 s are given in Figs. 1(a) and 1(b). After electrochemical deposition, the surface of the copper foam electrode was covered by a layer of mutually interconnected sheets. The thickness of these upstanding sheets was about 15 nm (Fig. 1(c)) and there was a continuous layer of 100–150 nm thickness below the upper

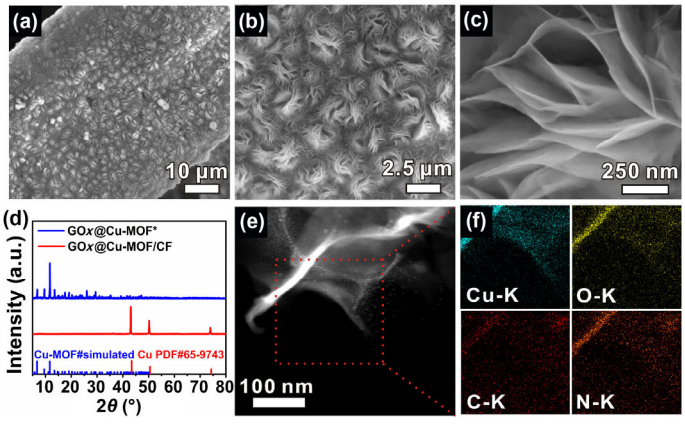

Figure 1 (a)–(c) SEM images of GO*x*@Cu-MOF layer growing on the copper foam substrate. (d) PXRD patterns of GO*x*@Cu-MOF/CF and GO*x*@Cu-MOF* exfoliated from the copper foam. (e) HAADF-STEM image of the exfoliated GO*x*@Cu-MOF sheet and (f) corresponding elemental mappings of Cu, O-K, C and N-K.

layer built with interconnected sheets (Fig. S2 in the ESM). PXRD patterns of the deposits exfoliated from the copper foam (denoted as GO*x*@Cu-MOF*) revealed the presence of Cu-based MOF (HKUST-1), but these peaks were almost undetectable in the PXRD pattern of GO*x*@Cu-MOF/CF (Fig. 1(d)). The presence of GO*x* was confirmed by EDX spectroscopy and corresponding elemental mappings recorded from an individual GOx@Cu-MOF* sheet. It can be clearly seen that all the elements uniformly distributed across the whole Cu-MOF zone (Figs. 1(e) and 1(f) and Fig. S3 in the ESM). Of note, the distribution status of N element that only originates from the amino acid groups of GO*x* is overlapped with that of O, C, and Cu, which constiute HKUST-1. Thus, the results indicate that a part of GO*x* was encapsulated in the bottom MOF layer near the surface of copper foam via electrostatic adsorption, and the rest of GO*x* was encapsulated within the upstanding Cu-MOF sheets via biomimetic mineralization, as illustrated in Scheme 1. Nevertheless, the immobilization of GO*x* had negligible effects on the growth of Cu-MOF (Fig. S4 in the ESM).

To further ascertain the characteristics of the encapsulation status of GO*x* within Cu-MOF, FTIR spectroscopy was performed. As shown in Fig. 2(a), GO*x*/Cu-MOF* showed obvious difference in color from GO*x*-free Cu-MOF* exfoliated from the copper foam. However, the FTIR spectra showed the appearance of peaks in the range of 1,380–1,630 cm^{-1}, which were characteristic of carboxylate group vibrations (Fig. 2(b)). Moreover, several low intensity peaks appeared at 1,710, 1,180, and 1,240 cm^{-1} corresponding to the vibrations of C=O, C–O and O–H groups, respectively. These results indicated that HKUST-1 Cu-MOF was successfully synthesized. The spectrum of GO*x* showed characteristic protein peaks at 1,640–1,660 and 1,510–1,560 cm^{-1}, corresponding to amide I (mainly from C=O stretching mode) and amide II bands (mainly from a combination of NH bending and CN stretching modes) [29]. However, no characteristic peaks of GO*x* appeared in the spectra of GO*x*@Cu-MOF*. These data clearly demonstrated that the mechanism of GO*x* encapsulation with Cu-MOF sheets was not via absorption or infiltration into the Cu-MOF pores, but via biomimetic mineralization [29].

In this study, the effects of various synthesis parameters (such as deposition potentials, deposition times, and concentration of precursors) on the architecture of the GO*x*@Cu-MOF/CF were systematically investigated in order to optimize the immobilization of GO*x* within Cu-MOF layers. At low deposition potential (1.00 V), the growth of Cu-MOF layer was restricted to the surface of copper foam, forming discrete bottom Cu-MOF layer zones (Fig. 3(a)). With the increase in deposition potential, bottom Cu-MOF layer zones gradually grew up, connecting each other, while some upstanding Cu-MOF sheets grew on the bottom Cu-MOF layer (Figs. 3(b)–3(d)). Accordingly, the quantity of GO*x* encapsulated significantly increased (Fig. S5 in the ESM). Similar morphology evolution trend was observed in the experiments with varying deposition time (Figs. 3(e)–3(h)) or varying concentration of organic ligands

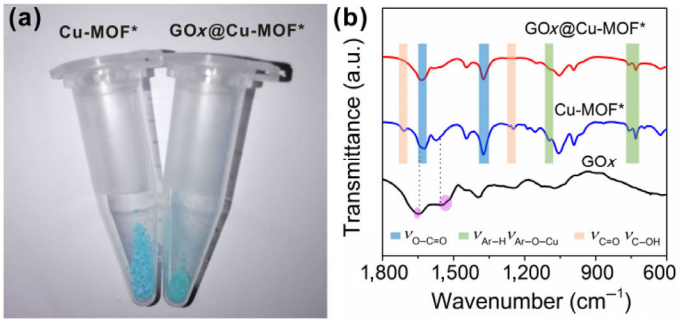

Figure 2 (a) Photographs of Cu-MOF* and GO*x*@Cu-MOF*. (b) FTIR spectra of GO*x*, Cu-MOF*, and GO*x*@Cu-MOF*.

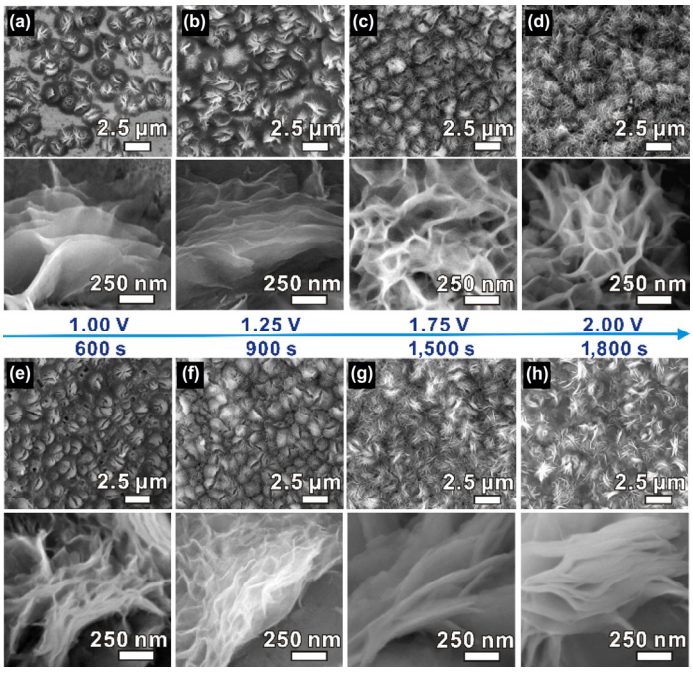

Figure 3 High magnification (upper) and low magnification (lower) SEM images of GO*x*@Cu-MOF/CF electrodes obtained with different (a) deposition potentials (1.00, 1.25, 1.75, and 2.00 V) or (b) deposition time (600, 900, 1,500, and 1,800 s). In deposition potential-dependent experiments, the deposition time was fixed at 1,200 s, and in deposition time-dependent experiments, the deposition potential was fixed at 1.50 V.

(Fig. S6 in the ESM). In contrast to other synthesis parameters, deposition potential had more significant impact on the formation of GO*x*@Cu-MOF on the copper foam. This is because the deposition potential directly controls the release rate of Cu^{2+} ions, thus affecting the growth rate of MOFs and the encapsulation of enzymes.

Based on above results, natural enzyme GO*x* was successfully immobilized on the 3D porous conducting electrode with the MOF encapsulation strategy. Such an architecture greatly guarantees efficient cascade between enzyme/nanozyme-catalyzed reactions and the sensitive signal acquisition, thereby leading to superior catalytic activity for glucose sensing (Fig. 4(a)). The bio-electrocatalytic detection of glucose over GO*x*@Cu-MOF/CF electrode was conducted in air-saturated 0.1 M phosphate buffered saline (PBS) solution at room temperature (25 °C). Figure 4(b) presents the CV curves of the representative electrode, which clearly shows that the reduction current increased with the successive addition of glucose. In the detection process of glucose, GO*x* embedded within Cu-MOF layer catalyzed glucose to gluconic acid and H_2O_2, and then Cu-MOF/CF electro-catalyzed the reduction of H_2O_2 immediately. The measurement results revealed that the electrode exhibited the optimal current response at –0.40 V (Fig. 4(c)). In addition, a well-defined linear relationship between the reduction current and the glucose concentration could be established in the concentration range from 0 to 6 mM (Fig. 4(d)). Strikingly, GO*x*@Cu-MOF/CF electrode had much higher sensitivity than the unprotected GO*x*/CF electrode. According to the Lineweaver-Burk plot (Fig. 4(e)), the apparent Michaelis constant (K_m) of the GO*x*@MOF/CF electrode was 0.51 mM, much lower than those previously reported for free GO*x* (25.7 mM) or MOF encapsulated GO*x* (~ 39 mM) [39]. The lower K_m value for the GO*x*@MOF/CF electrode reveals its better affinity for glucose and thus, contributes to its high sensitivity for glucose detection.

The significantly improved glucose sensitivity of GO*x*@MOF/CF electrode could be understood from two aspects. On one hand, high local concentrations of substrates/products are easily generated in such a confined environment within Cu-MOF layer. On the other hand, there are no diffusion barriers for the permeation of the

Nano Res. 2019, 12(12): 3031–3036

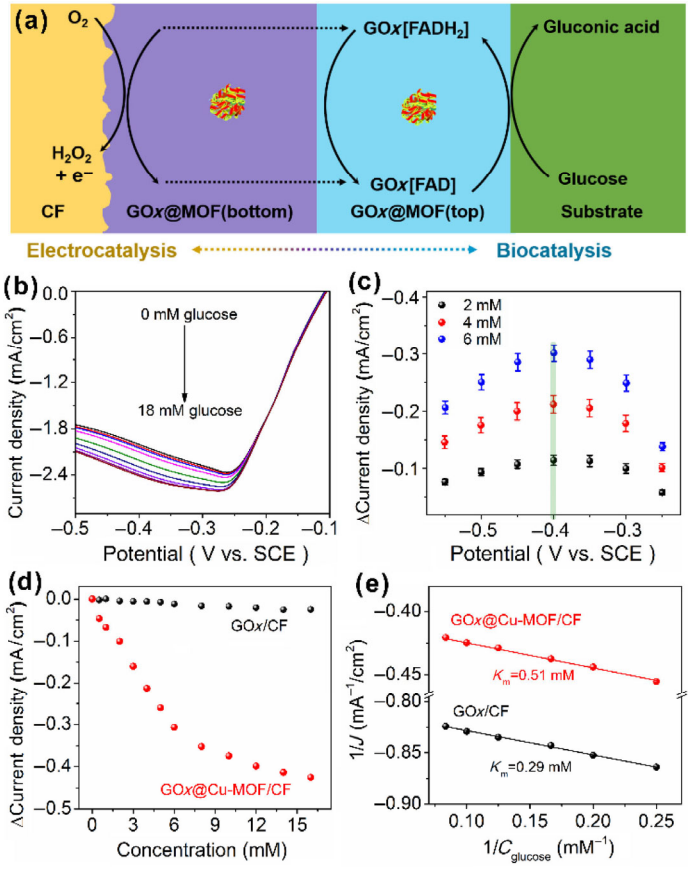

Figure 4 (a) Schematic illustration of the bio-electrocatalytic cascade reaction mechanism over GO*x*@Cu-MOF/CF towards glucose sensing. (b) CVs corresponding to different glucose concentrations. (c) Effect of applied potentials on the amperometric response of 2, 4, and 6 mM glucose. (d) Calibration plots derived from the CVs at −0.40 V vs. SCE. (e) Lineweaver-Burk plots of GO*x*@Cu-MOF/CF and GO*x*/CF electrodes derived from (d) within concentration range of 4–12 mM.

substrates into Cu-MOF or for the release of the product from Cu-MOF. These two factors greatly increase the cascade efficiency of enzyme catalyzed process and electro-catalyzed process [5, 16]. Of note, it was found that the sensitivity of GO*x*@Cu-MOF modified electrode increased first and then decreased as deposition potentials, times, or concentrations of BTC increased (Figs. 5(a)–5(c)). This is because an excessively thick GO*x*@Cu-MOF layer would affect the diffusion of substrates and products, resulting in the decrease in sensitivity. In addition to the diffusion problem, the aggregation of enzyme caused by high concentration could also inhibit the activity of GO*x* (Fig. 5(d)) [39].

It is well known that enzymes can be easily deactivated by any abrupt changes in their external environment (typically heat). Therefore, stability of immobilized enzyme is an important problem which has to be solved before practical applications. For this purpose, the heat-resistance of GO*x*@MOF/CF was specifically investigated herein. As revealed in Fig. 6(a), the activity of GO*x*@Cu-MOF modified electrode barely decreased (< 2%) when it was incubated in water for 1 h at 40 °C. Surprisingly, the electrode still retained ca. 80% of its initial activity after it was incubated at 80 °C. In contrast, the activity of un-encapsulated GO*x*/CF quickly declined with the increase in incubation temperature (Fig. 6(b)). At 40 °C, the un-encapsulated GO*x*/CF electrode lost over half of its original activity, while its activity at 80 °C was drastically reduced to below 10% of the original value.

In general, the thicker the MOF layer, the better its protective effect on the encapsulated GO*x*, which was confirmed by the deposition potential-dependent experiments (Fig. 6(c)). At low deposition potentials, as-formed Cu-MOF layers could not completely cover

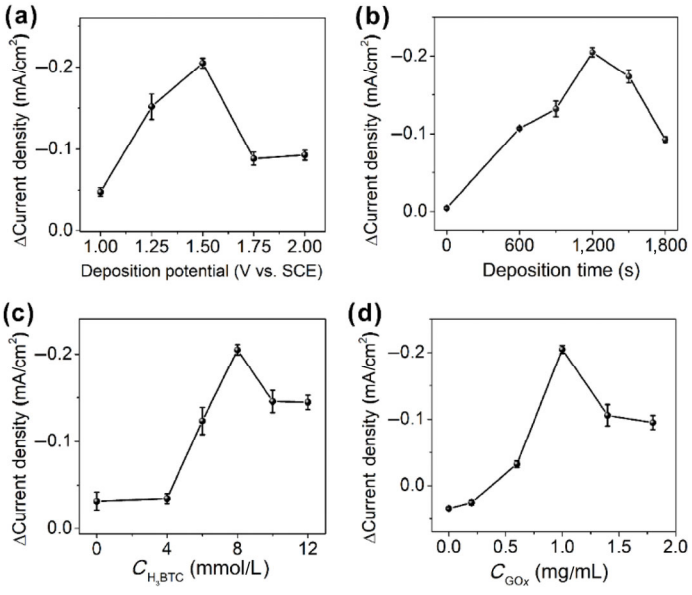

Figure 5 Effects of different experimental conditions on electro-catalytic activity of electrode. (a) deposition potential, (b) deposition time, (c) concentration of BTC, (d) concentration of GO*x*.

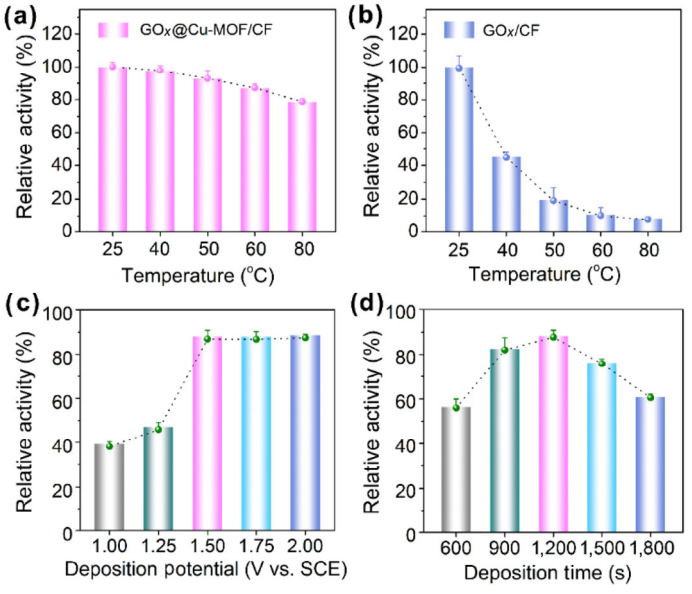

Figure 6 Activity retention rates of (a) GO*x*@MOF/CF and (b) GO*x*/CF incubated in water at different temperatures for 1 h. Thermal stability of the GO*x*@MOF/CF electrodes deposited (c) at different potentials for 1,200 s and (d) at 1.5 V for different time, which were incubated in water for 1 h at 60 °C.

the immobilized GO*x* on copper foam due to limited dissolution of Cu^{2+} ions (Figs. 3(a) and 3(b)). Under these conditions, the exposed GO*x* regions were not protected from high temperature by the Cu-MOF layer. With the increase in deposition potential, the degree of coverage of GO*x* increased significantly, and the thermal stability was improved accordingly. When the Cu-MOF layer was thick enough to encapsulate GO*x* to shield it from high temperature, further increase in Cu-MOF layer thickness did not enhance the thermal stability. Furthermore, the deposition time also had different effects on the thermal stability of GO*x*@Cu-MOF modified electrode (Fig. 6(d)). For the GO*x*@Cu-MOF modified electrodes obtained at long deposition times, thermal stability became worse, which was likely due to the incomplete encapsulation of GO*x* by MOF layer.

Table 1 is the comparison of the performance of the GO*x*@Cu-MOF/CF with that of other previously reported immobilized enzyme sensors [39–45]. For the GO*x*@Cu-MOF/CF, there is no diffusion

Table 1 Comparison of the performance of the proposed GO*x*@Cu-MOF/CF with other immobilized enzyme modified electrode

Sensing materials	Enzyme	*K*m (mM)	Relative activity (%)	Ref.
GO*x*&CuBDC	GO*x*	37.8	80 (80 °C)	[39]
PGA@SNF@ZIF-8	PGA	106.1	90 (60 °C)	[40]
GO*x*@CHNs	GO*x*	14.39	—	[41]
n-ZnPc-co-TP/GO*x*	GO*x*	2.721	—	[42]
Nafion/GO*x*-yeast/MWNTs	GO*x*	—	41 (60 °C)	[43]
GO*x*-HRP@DM@MP	GO*x*-HRP	1.41	32 (80 °C)	[44]
chitosan/GO*x*/ZnO/Au	GO*x*	1.09	—	[45]
GO*x*@Cu-MOF/CF	GO*x*	0.51	86 (60 °C)/ 81 (80 °C)	This work

barrier for substrates to activity sites of enzymes within Cu-MOF nanosheets, compared with bulk MOFs or hydrophobic MOFs [39, 40]. This contributes to the affinity of substrate to enzyme, resulting in lower K_m of GO*x*@Cu-MOF/CF. As for the proposed encapsulation method, the enzymes embeded within the MOF matrices have better thermal stability than those immobilized onto the matrices such as carbon nanotubes due to the protection of MOF shell [41–45]. In a word, the proposed GO*x*@Cu-MOF/CF sensor exhibited better affinity to glucose and thermal stability benefitting from the preparation method of Cu-MOF nanosheets grown around GO*x* via the biomimetic mineralization.

The stability of GO*x*@Cu-MOF modified electrode was also studied by using SEM. The surface of the copper foam electrode was still covered completely by a layer of upstanding nanosheets after incubated in water at 80 °C for 1 h and subsequent test reaction (Fig. 7(a)). From the high-magnification SEM images of the GO*x*@Cu-MOF (Figs. 7(b) and 7(c)), there was no damage found on the surface of nanosheets. These data further conformed the excellent thermal stability of GO*x*@Cu-MOF modified electrode. This MOF encapsulated enzyme structure can be potentially applied for efficient photo-thermal therapy and other platforms subjected to harsh operating conditions.

4 Conclusions

In summary, this work demonstrated the one-step synergetic fabrication of GO*x*@Cu-MOF modified copper foam multienzyme system through electrochemical oxidation and biomimetic mineralization, and its use as a glucose sensing electrode. This construction process is under moderate conditions (room temperature), significantly reducing damage to enzymes. The open porous structure of copper foam electrode allows the substrates access to the sensing sites, while the MOF layer provides good protection for GO*x* embedded inside. The as-prepared electrode exhibited significantly enhanced sensitivity and thermal stability in glucose sensing because the electrode design facilitated the cascade catalytic process between GO*x*-catalyzed glucose oxidation and electro-catalyzed H_2O_2 reduction. Therefore, this work offers a simple synthetic route to immobilize specific enzymes. Considering its high stability, this MOF encapsulated enzyme structure can be potentially applied for efficient photo-thermal therapy and other platforms subjected to harsh operating conditions.

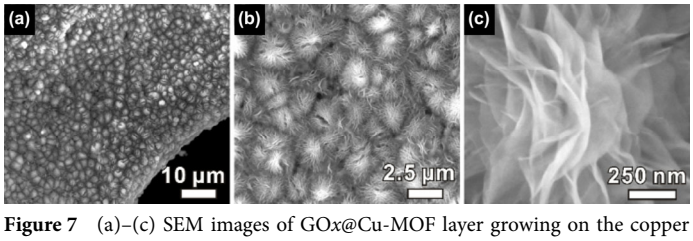

Figure 7 (a)–(c) SEM images of GO*x*@Cu-MOF layer growing on the copper foam substrate incubated in water at 80 °C for 1 h and then after reaction.

Acknowledgements

This work was supported by the National Key Research and Development Program of China (Nos. 2017YFA0206500 and 2017YFA0206801), the National Basic Research Program of China (No. 2015CB932301), and the National Natural Science Foundation of China (Nos. 21671163, 21721001, and J1310024).

Electronic Supplementary Material: Supplementary material (SEM images of bare copper foam and GO*x* modified copper foam, SEM image of GO*x*@Cu-MOF deposited at 1.25 V for 1,200 s and corresponding EDX element mapping images, XRD patterns of Cu-MOF* and GO*x*@Cu-MOF* exfoliated from the copper foams, elemental analysis by SEM-EDS of GO*x*@Cu-MOF/CF electrodes obtained with different deposition potential, SEM images of GO*x*@Cu-MOF/CF electrodes obtained with different concentrations of BTC) is available in the online version of this article at https://doi.org/10.1007/s12274-019-2548-8.

References

[1] Bornscheuer, U. T.; Huisman, G. W.; Kazlauskas, R. J.; Lutz, S.; Moore, J. C.; Robins, K. Engineering the third wave of biocatalysis. *Nature* **2012**, *485*, 185–194.

[2] Turner, N. J. Directed evolution drives the next generation of biocatalysts. *Nat. Chem. Biol.* **2009**, *5*, 567–573.

[3] Trifonov, A.; Tel-Vered, R.; Fadeev, M.; Willner, I. Electrically contacted bienzyme-functionalized mesoporous carbon nanoparticle electrodes: Applications for the development of dual amperometric biosensors and multifuel-driven biofuel cells. *Adv. Energy Mater.* **2015**, *5*, 1401853.

[4] Geng, P. B.; Zheng, S. S.; Tang, H.; Zhu, R. M.; Zhang, L.; Cao, S.; Xue, H. G.; Pang. H. Transition metal sulfides based on graphene for electrochemical energy storage. *Adv. Energy Mater.* **2018**, *8*, 1703259.

[5] Chen, W. H.; Vázquez-González, M.; Zoabi, A.; Abu-Reziq, R.; Willner, I. Biocatalytic cascades driven by enzymes encapsulated in metal–organic framework nanoparticles. *Nat. Catal.* **2018**, *1*, 689–695.

[6] Feng, D. W.; Liu, T. F.; Su, J.; Bosch, M.; Wei, Z. W.; Wan, W.; Yuan, D. Q.; Chen, Y. P.; Wang, X.; Wang, K. C. et al. Stable metal-organic frameworks containing single-molecule traps for enzyme encapsulation. *Nat. Commun.* **2015**, *6*, 5979.

[7] Zhang, C.; Wang, X. R.; Hou, M.; Li, X. Y.; Wu, X. L.; Ge, J. Immobilization on metal–organic framework engenders high sensitivity for enzymatic electrochemical detection. *ACS Appl. Mater. Interfaces* **2017**, *9*, 13831–13836.

[8] Wang, Q. Q.; Zhang, X. P.; Huang, L.; Zhang, Z. Q.; Dong, S. J. GO*x*@ZIF-8 (NiPd) nanoflower: An artificial enzyme system for tandem catalysis. *Angew. Chem., Int. Ed.* **2017**, *56*, 16082–16085.

[9] Wei, H.; Wang, E. K. Nanomaterials with enzyme-like characteristics (nanozymes): Next-generation artificial enzymes. *Chem. Soc. Rev.* **2013**, *42*, 6060–6093.

[10] Lian, X. Z.; Chen, Y. P.; Liu, T. F.; Zhou, H. C. Coupling two enzymes into a tandem nanoreactor utilizing a hierarchically structured MOF. *Chem. Sci.* **2016**, *7*, 6969–6973.

[11] Lian, X. Z.; Erazo-Oliveras, A.; Pellois, J. P.; Zhou, H. C. High efficiency and long-term intracellular activity of an enzymatic nanofactory based on metal-organic frameworks. *Nat. Commun.* **2017**, *8*, 2075.

[12] Zheng, S. S.; Xue, H. G.; Pang, H. Supercapacitors based on metal coordination materials. *Coord. Chem. Rev.* **2018**, *373*, 2–21.

[13] Vijayalakshmi, A.; Karthikeyan, R.; Berchmans, S. Nonenzymatic reduction of hydrogen peroxide produced during the bioelectrocatalysis of glucose oxidase on urchin-like nanofibrillar structures of Cu on Au substrates. *J. Phys. Chem. C* **2010**, *114*, 22159–22164.

[14] Lee, S.; Ringstrand, B. S.; Stone, D. A.; Firestone, M. A. Electrochemical activity of glucose oxidase on a poly(ionic liquid)–Au nanoparticle composite. *ACS Appl. Mater. Interfaces* **2012**, *4*, 2311–2317.

[15] Ma, W. J.; Jiang, Q.; Yu, P.; Yang, L. F.; Mao, L. Q. Zeolitic imidazolate framework-based electrochemical biosensor for *in vivo* electrochemical measurements. *Anal. Chem.* **2013**, *85*, 7550–7757.

[16] Zhang, Y. F.; Ge, J.; Liu, Z. Enhanced activity of immobilized or chemically modified enzymes. *ACS Catal.* **2015**, *5*, 4503–4513.

[17] Doonan, C.; Ricco, R.; Liang, K.; Bradshaw, D.; Falcaro, P. Metal–organic frameworks at the biointerface: Synthetic strategies and applications. *Acc. Chem. Res.* **2017**, *50*, 1423–1432.
[18] Lian, X. Z.; Fang, Y.; Joseph, E.; Wang, Q.; Li, J. L.; Banerjee, S.; Lollar, C.; Wang, X.; Zhou, H. C. Enzyme–MOF (metal–organic framework) composites. *Chem. Soc. Rev.* **2017**, *46*, 3386–3401.
[19] Mehta, J.; Bhardwaj, N.; Bhardwaj, S. K.; Kim, K. H.; Deep, A. Recent advances in enzyme immobilization techniques: Metal-organic frameworks as novel substrates. *Coord. Chem. Rev.* **2016,** *322*, 30–40.
[20] Gkaniatsou, E.; Sicard, C.; Ricoux, R.; Benahmed, L.; Bourdreux, F.; Zhang, Q.; Serre, C.; Mahy, J. P.; Steunou, N. Enzyme encapsulation in mesoporous metal–organic frameworks for selective biodegradation of harmful dye molecules. *Angew. Chem., Int. Ed.* **2018**, *57*, 16141–16146.
[21] Hanefeld, U.; Gardossi, L.; Magner, E. Understanding enzyme immobilisation. *Chem. Soc. Rev.* **2009**, *38*, 453–468.
[22] Kempahanumakkagari, S.; Kumar, V.; Samaddar, P.; Kumar, P.; Ramakrishnappa, T.; Kim, K. H. Biomolecule-embedded metal-organic frameworks as an innovative sensing platform. *Biotechnol. Adv.* **2018**, *36*, 467–481.
[23] Gkaniatsou, E.; Sicard, C.; Ricoux, R.; Mahy, J. P.; Steunou, N.; Serre, C. Metal–organic frameworks: A novel host platform for enzymatic catalysis and detection. *Mater. Horiz.* **2017**, *4*, 55–63.
[24] Chen, L. N.; Zhan, W. W.; Fang, H. H.; Cao, Z. M.; Yuan, C. F.; Xie, Z. X.; Kuang, Q.; Zheng, L. S. Selective catalytic performances of noble metal nanoparticle@MOF composites: The concomitant effect of aperture size and structural flexibility of MOF matrices. *Chem.—Eur. J.* **2017**, *23*, 11397−33403.
[25] Chen, L. N.; Zhang, X. B.; Zhou, J. H.; Xie, Z. X.; Kuang, Q.; Zheng, L. S. A Nano-reactor based on PtNi@metal–organic framework composites loaded with polyoxometalates for hydrogenation–esterification tandem reactions. *Nanoscale* **2019**, *11*, 3292−3299.
[26] Xu, W. Q.; Jiao, L.; Yan, H. Y.; Wu, Y.; Chen, L. J.; Gu, W. L.; Du, D.; Lin, Y. H.; Zhu, C. Z. Glucose oxidase-integrated metal–organic framework hybrids as biomimetic cascade nanozymes for ultrasensitive glucose biosensing. *ACS Appl. Mater. Interfaces* **2019**, *11*, 22096–22101.
[27] Chen, G. S.; Huang, S. M.; Kou, X. X.; Wei, S. B.; Huang, S. Y.; Jiang, S. Q.; Shen, J.; Zhu, F.; Ouyang, G. F. A convenient and versatile amino-acid-boosted biomimetic strategy for the nondestructive encapsulation of biomacromolecules within metal−organic frameworks. *Angew. Chem., Int. Ed.* **2019**, *58*, 1463–1467.
[28] Cowan, D. A.; Fernandez-Lafuente, R. Enhancing the functional properties of thermophilic enzymes by chemical modification and immobilization. *Enzyme Microb. Technol.* **2011**, *49*, 326−346.
[29] Liang, K.; Ricco, R.; Doherty, C. M.; Styles, M. J.; Bell, S.; Kirby, N.; Mudie, S.; Haylock, D.; Hill, A. J.; Doonan, C. J. et al. Biomimetic mineralization of metal-organic frameworks as protective coatings for biomacromolecules. *Nat. Commun.* **2015**, *6*, 7240.
[30] Li, P.; Modica, J. A.; Howarth, A. J.; Vargas L, E.; Moghadam, P. Z.; Snurr, R. Q.; Mrksich, M.; Hupp, J. T.; Farha, O. K. Toward design rules for enzyme immobilization in hierarchical mesoporous metal-organic frameworks. *Chem* **2016**, *1*, 154−169.
[31] Chen, L. N.; Wang, T.; Xue, Y. K.; Zhou, X.; Zhou, J. H.; Cheng, X. Q.; Xie, Z. X.; Kuang, Q.; Zheng, L. S. Rationally armoring PtCu alloy with metal-organic frameworks as highly selective nonenzyme electrochemical sensor. *Adv. Mater. Interfaces* **2018**, *5*, 1801168.
[32] Mohammad, M.; Razmjou, A.; Liang, K.; Asadnia, M.; Chen, V. Metal–organic-framework-based enzymatic microfluidic biosensor via surface patterning and biomineralization. *ACS Appl. Mater. Interfaces* **2019**, *11*, 1807–1820.
[33] Qiu, Q. M.; Chen, H. Y.; Wang, Y. X.; Ying, Y. B. Recent advances in the rational synthesis and sensing applications of metal-organic framework biocomposites. *Coord. Chem. Rev.* **2019**, *387*, 60–78.
[34] Zhang, Y. F.; Hess, H. Toward rational design of high-efficiency enzyme cascades. *ACS Catal.* **2017**, *7*, 6018–6027.
[35] Wang, M.; Mohanty, S. K.; Mahendra, S. Nanomaterial-supported enzymes for water purification and monitoring in point-of-use water supply systems. *Acc. Chem. Res.* **2019**, *52*, 876–885.
[36] Campagnol, N.; Stassen, I.; Binnemans, K.; De Vos, D. E.; Fransaer, J. Metal–organic framework deposition on dealloyed substrates. *J. Mater. Chem. A* **2015**, *3*, 19747−19753.
[37] Li, W. J.; Tu, M.; Cao, R.; Fischer, R. A. Metal−organic framework thin films: Electrochemical fabrication techniques and corresponding applications & perspectives. *J. Mater. Chem. A* **2016**, *4*, 12356−12369.
[38] Campagnol, N.; Van Assche, T. R. C.; Li, M. Y.; Stappers, L.; Dincă, M.; Denayer, J. F. M.; Binnemans, K.; De Vos, D. E.; Fransaer, J. On the electrochemical deposition of metal–organic frameworks. *J. Mater. Chem. A* **2016**, *4*, 3914−3925.
[39] Li, Z. X.; Xia, H.; Li, S. M.; Pang, J. F.; Zhu, W.; Jiang Y. B. *In situ* hybridization of enzymes and their metal–organic framework analogues with enhanced activity and stability by biomimetic mineralisation. *Nanoscale* **2017**, *9*, 15298–15302.
[40] Du, Y. J.; Gao, J.; Liu, H. J.; Zhou, L. Y.; Ma, L.; He, Y.; Huang, Z. H.; Jiang, Y. J. Enzyme@silica nanoflower@metal-organic framework hybrids: A novel type of integrated nanobiocatalysts with improved stability. *Nano Res.* **2018**, *11*, 4380–4389.
[41] Li, Z. X.; Ding, Y.; Li, S. M.; Jiang, Y. B.; Liu Z.; Ge J. Highly active, stable and self-antimicrobial enzyme catalysts prepared by biomimetic mineralization of copper hydroxysulfate. *Nanoscale* **2016**, *8*, 17440–17445.
[42] Soganci, T.; Baygu, Y.; Kabay, N.; Gök, Y.; Ak, M. Comparative investigation of peripheral and nonperipheral zinc phthalocyanine-based polycarbazoles in terms of optical, electrical, and sensing properties. *ACS Appl. Mater. Interfaces* **2018**, *10*, 21654–21665.
[43] Wang, H. W.; Lang, Q. L.; Li, L.; Liang, B.; Tang, X. J.; Kong, L. R.; Mascini, M.; Liu, A. H. Yeast surface displaying glucose oxidase as whole-cell biocatalyst: Construction, characterization, and its electrochemical glucose sensing application. *Anal. Chem.* **2013**, *85*, 6107–6112.
[44] Yang, Y.; Zhang, R. Q.; Zhou, B. N.; Song, J. Y.; Su, P.; Yang, Y. High activity and convenient ratio control: DNA-directed coimmobilization of multiple enzymes on multifunctionalized magnetic nanoparticles. *ACS Appl. Mater. Interfaces* **2017**, *9*, 37254–37263.
[45] Zhao, M. G.; Li, Z. L.; Han, Z. Q.; Wang, K.; Zhou, Y.; Huang, J. Y.; Ye, Z. Z. Synthesis of mesoporous multiwall ZnO nanotubes by replicating silk and application for enzymatic biosensor. *Biosens. Bioelectron.* **2013**, *49*, 318–322.